Thermodynamics and kinetics of lithiation-induced phase transitions in nanoporous antimony

Shichen Wang[a], Zeyu Jin[a], Chaojie Yang[a], Jie Lu[a], Yao Gao[b], Huajun Qiu[a,*], Kaikai Li[a,*]

[a] School of Materials Science and Engineering, Harbin Institute of Technology, Shenzhen, 518055, China.

[b] Department of physics, the Chinese University of Hong Kong, Shatin, New Territories, Hong Kong.

[*] Email: likaikai@hit.edu.cn

[*] Email: qiuhuajun@hit.edu.cn

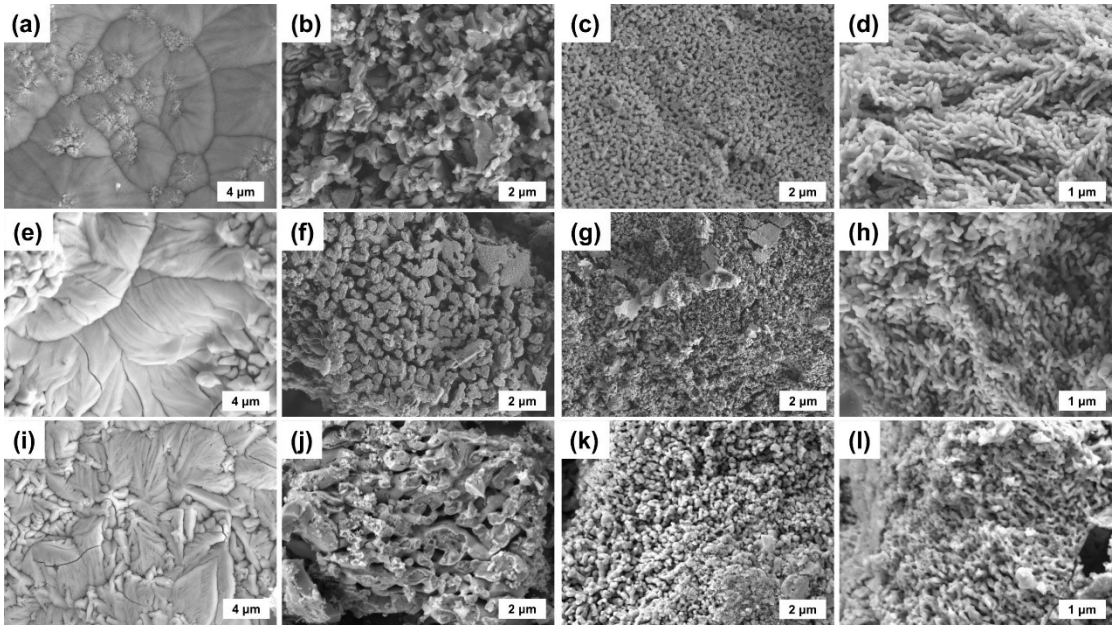

Figure S1. SEM images of the process of formation of nanoporous structure of precursor alloy. a) SEM image of $Al_{85}Sb_{15}$ alloy ribbon. b-d) SEM images of $Al_{85}Sb_{15}$ alloy ribbon immersed in the NaOH solution for 1 h, 6 h and 12 h, respectively. e) SEM image of $Al_{80}Sb_{20}$ alloy ribbon. f-h) SEM images of $Al_{80}Sb_{20}$ alloy ribbon immersed in the NaOH solution for 1 h, 6 h and 12 h, respectively. i) SEM image of $Al_{70}Sb_{30}$ alloy ribbon. j-l) SEM images of $Al_{70}Sb_{30}$ alloy ribbon immersed in the NaOH solution for 1 h, 6 h and 12 h, respectively.

The nanoporous Sb samples were prepared through the dealloying of Sb-Al precursor alloys. We synthesized three precursor alloys with distinct ratios by adjusting the quantities of aluminum and Sb during the alloying process. Based on the principle that Sb is inert to NaOH aqueous solution at room temperature, whereas Al reacts readily with it, Al was employed as a sacrificial element to produce monolithic antimony with a nanoporous structure. The reaction mechanism of Al with an excess of NaOH aqueous solution is shown in the following equation:

$$2Al + 2NaOH + 6H_2O \rightarrow 2Na[(AlOH)_4] + 3H_2\uparrow \quad (1)$$

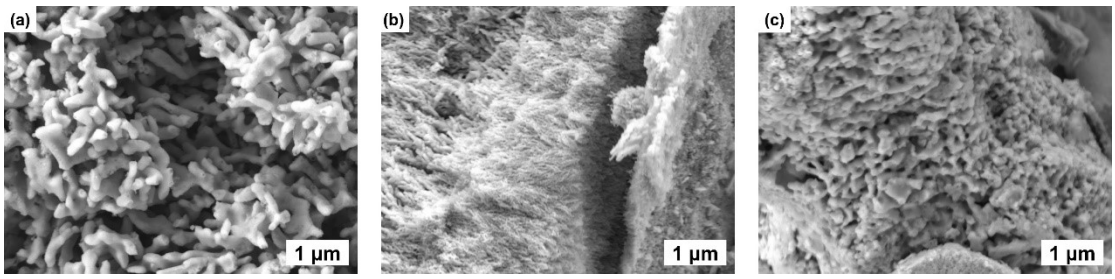

Figure S2. SEM images of a) Sb-15, b) Sb-20, and c) Sb-30.

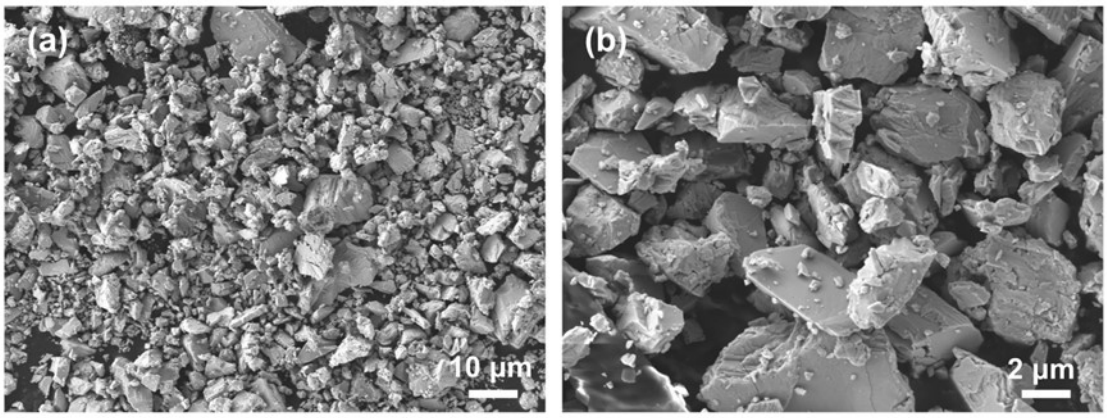

Figure S3. SEM images of Bulk Sb.

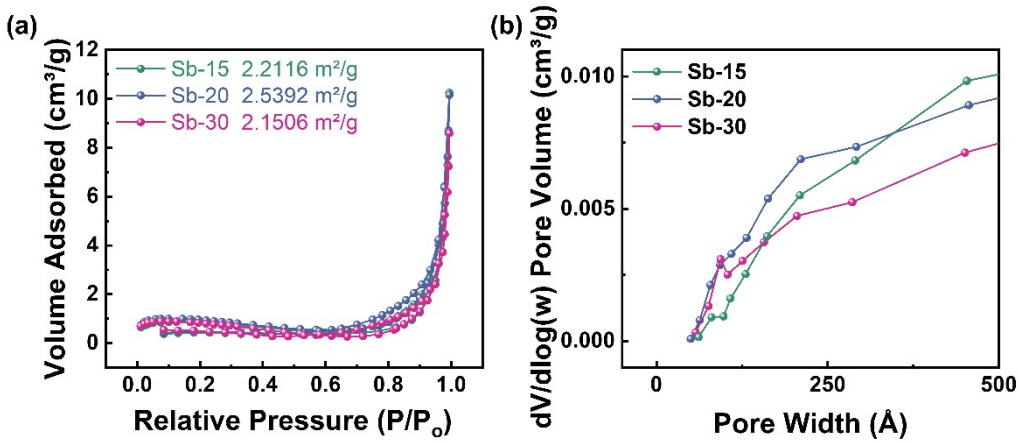

Figure S4. a) N_2 adsorption-desorption isotherms. b) Pore-size distribution curves.

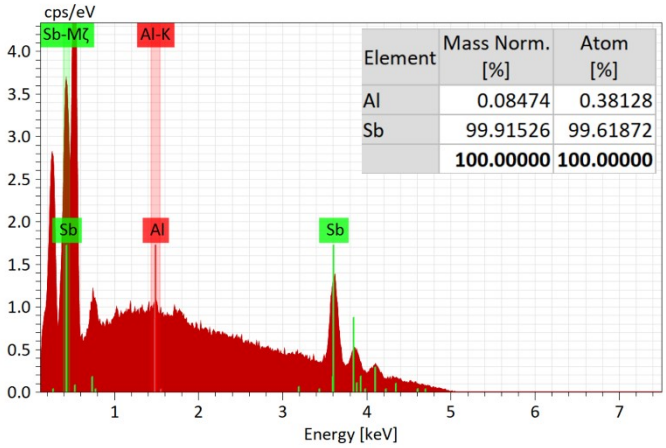

Figure S5. EDX spectrum of Sb-20 and percentage of elements.

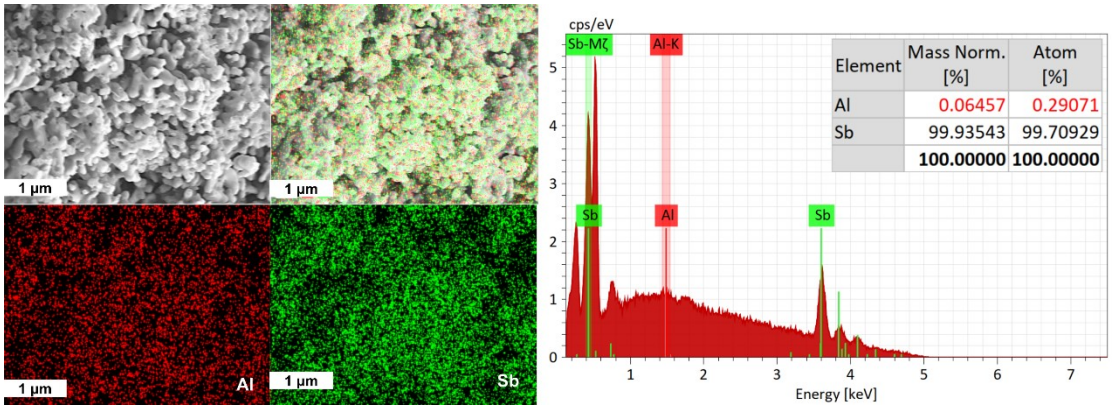

Figure S6. EDX spectrum of Sb-15 and elemental mapping showing the presence of Al and Sb as major elements.

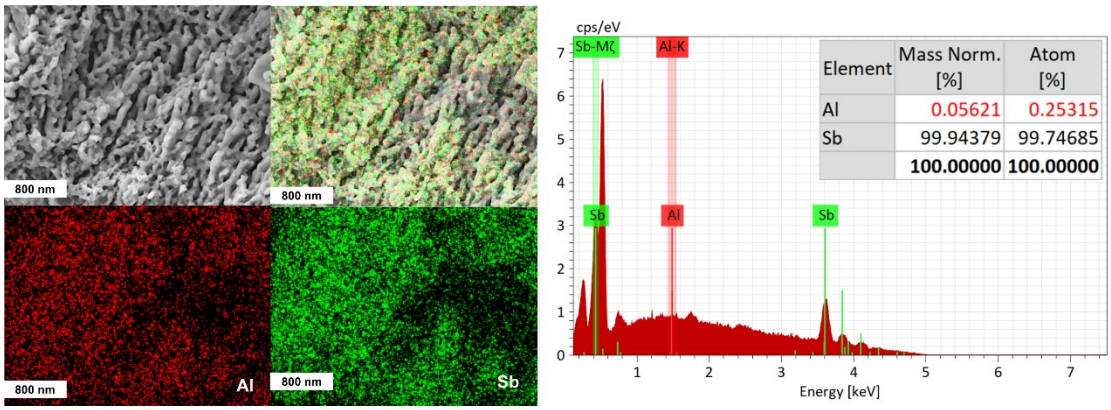

Figure S7. EDX spectrum of Sb-30 and elemental mapping showing the presence of Al and Sb as major elements.

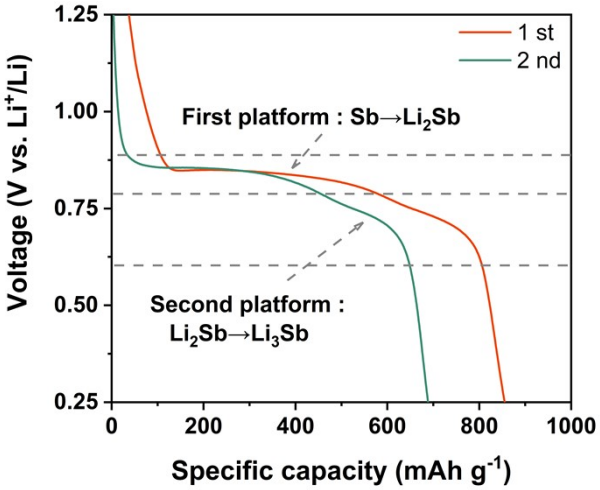

Figure S8. The discharge curves of Sb-20 electrode.

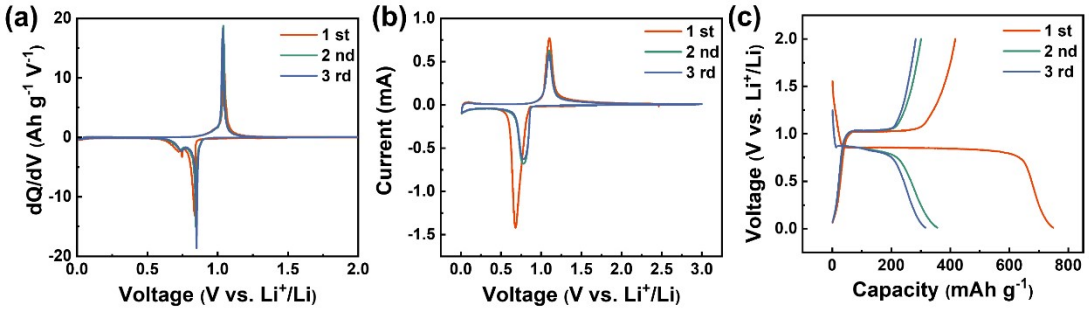

Figure S9. a) The corresponding dQ/dV curves of Sb-20. b) CV curves of Bulk Sb at a scan rate of 0.1 mV s^{-1}. c) Galvanostatic charge-discharge curves of Bulk Sb at a current density of 0.15 C.

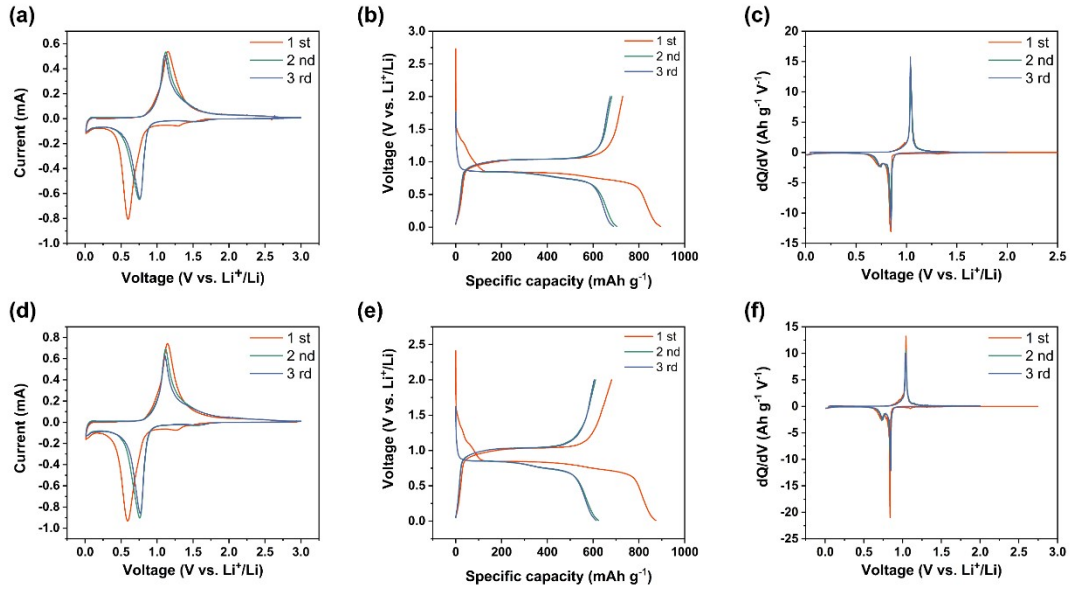

Figure S10. a) CV curves of Sb-15 at a scan rate of 0.1 mV s^{-1}. b) Galvanostatic charge-discharge curves of Sb-15 at a current density of 0.1 C. c) The corresponding dQ/dV curves of Sb-15. d) CV curves of Sb-30 at a scan rate of 0.1 mV s^{-1}. e) Galvanostatic charge-discharge curves of Sb-30 at a current density of 0.1 C. f) The corresponding dQ/dV curves of Sb-30.

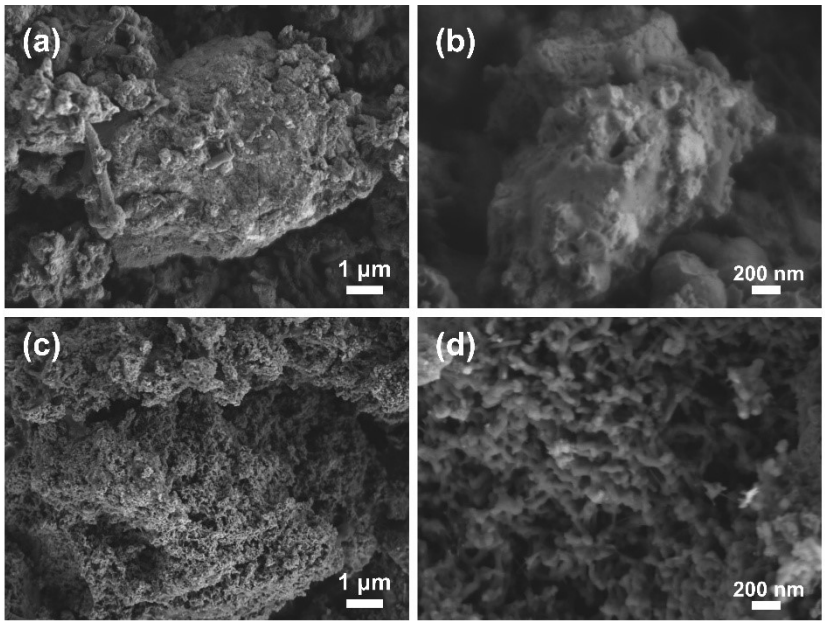

Figure S11. Postmortem characterization of a, b) Bulk Sb and c, d) Sb-20 after the 200th cycle at a current density of 0.5 C.

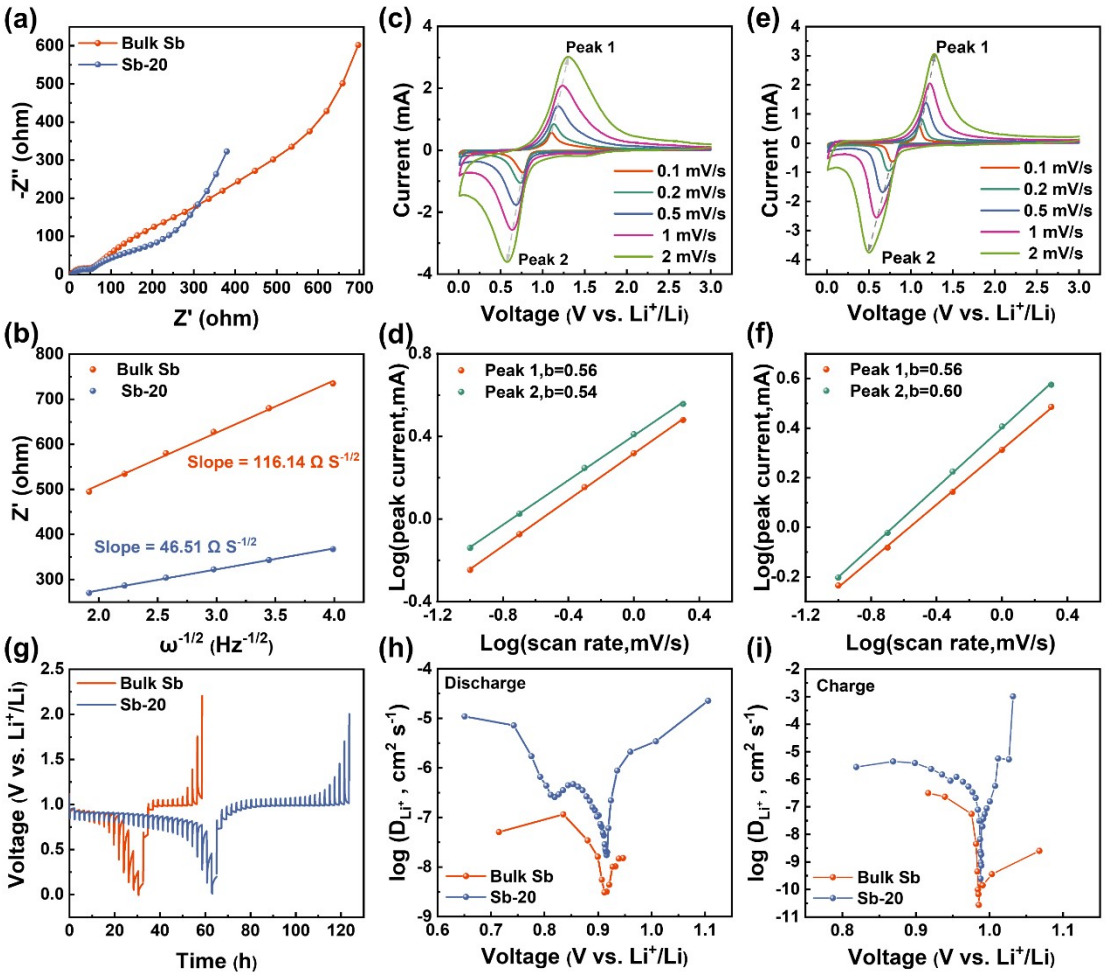

Figure S12. a) Nyquist plots for Bulk Sb and Sb-20, and b) corresponding $Z' - \omega^{-1/2}$ plots. c) CV curves of Sb-20 at different scan rates and d) the corresponding plot of log(*i*) versus log (*v*). e) CV curves of Bulk Sb at different scan rates and f) the corresponding plot of log(*i*) versus log (*v*). g) The GITT curves of the Sb-20 and Bulk Sb. h-i) The diffusion coefficient of Li^+ during h) discharge and i) charge process of Sb-20 and Bulk Sb.

Insights into the lithium-ion diffusion kinetics in different electrode materials were revealed using electrochemical impedance spectroscopy (EIS), cyclic voltammetry (CV), and galvanostatic intermittent titration technique (GITT). **Figure S12a** presents the Nyquist plots for Bulk Sb and Sb-20 electrodes after three cycles at a current density of 0.1 C, with both electrodes exhibiting the same trend. Each spectrum comprises two semicircles and a slope, corresponding to the electrode-electrolyte interface impedance (R_{sei}) in the high-frequency region, the charge transfer resistance (R_{ct}) in the medium-frequency region, and the ion diffusion impedance in the low-frequency region, respectively. We employed the equivalent circuit diagram shown in **Figure S13** for fitting to obtain the R_{sei} and R_{ct} values. As shown in **Table S1**, the R_{sei} values for Bulk Sb and Sb-20 electrodes are 39.9 Ω and 34.36 Ω, respectively, while the R_{ct} values are 93.87 Ω and 49.34 Ω, respectively. Both

R_{sei} and R_{ct} of the Sb-20 electrode are smaller than those of Bulk Sb. The corresponding slope related to the Warburg impedance (W_0) represents the Li^+ transfer process within the electrode material. The Warburg coefficient, a metric of Li^+ diffusion kinetics, can be inferred from the slope of $Z' - \omega^{-1/2}$ in the low-frequency region (**Figure S12b**). In this case, the calculated slope for Sb-20 is 46.51 Ω $S^{-1/2}$, which is smaller than that of Bulk Sb (116.14 Ω $S^{-1/2}$), indicating a significant improvement in ion transport capability for Sb-20.

The diffusion behavior of lithium-ion in Sb-20 electrode was also assessed through CV curves at various scanning rates, as depicted in **Figure S12c**. In CV analysis, the relationship between the scan rate (v) and peak current (i) follows the power law equation,

$$i = av^b \tag{2}$$

where a and b are adjustable coefficients. A b-value of 0.5 indicates a response that is primarily diffusion-controlled, while a b-value of 1.0 indicates a behavior that is primarily surface-influenced.[27] Fitting $log(i)$ vs $log(v)$ (**Figure S12d**) reveals that the b-values for Peak 1 and Peak 2 are 0.56 and 0.54, respectively. This suggests that the lithium-ion diffusion in Sb-20 electrode is diffusion-controlled. The CV test results for Bulk Sb, Sb-15, and Sb-30, shown in **Figures S12e-f** and **Figure S14**, are like those of the Sb-20 electrodes, which are mainly controlled by diffusion (**Table S2**). GITT was further conducted to calculate the Li-ion diffusion coefficient in Bulk Sb and Sb-20 electrodes (**Figure S12g**). The Li^+ diffusion coefficient ($D_{Li-GITT}$) values at various voltages were computed using Fick's second law of diffusion, as expressed in the abbreviated equation below,[20]

$$D_{Li-GITT} = \frac{4}{\pi\tau}\left(\frac{n_m V_m}{A}\right)^2\left(\frac{\Delta E_s}{\Delta E_\tau}\right)^2 \tag{3}$$

τ (s) represents the pulse duration, n_m (mol) and V_m (cm^3 mol^{-1}) denote the moles number and molar volume of Sb, and A (cm^2) represents the contact area between the electrode and electrolyte. ΔE_s and ΔE_τ represent the voltage variation during the current pulse and the equilibrium-state potential alteration. As shown in **Figure S12h-i**, the Sb-20 electrode exhibits larger average diffusion coefficients than Bulk Sb. This supports the notion that the Sb-20 electrode, with its smaller sized coral-like three-dimensional network and denser nanopores, demonstrates superior ion transport kinetics. In summary, we can conclude that the Sb-20 electrode exhibits superior diffusion kinetics

compared to the Bulk Sb electrode.

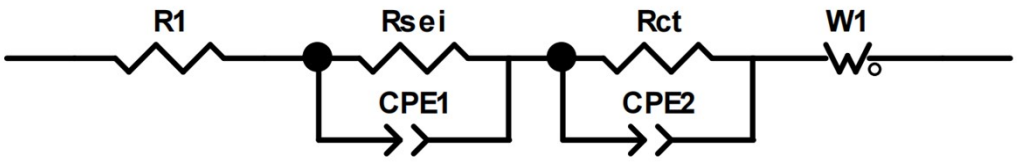

Figure S13. Equivalent electrical circuits used for analysis of EIS data.

Table S1. Fitting results obtained from the EIS data in **Figure 3a**.

	R_e (Ω)	R_{sei} (Ω)	R_{ct} (Ω)
Bulk Sb	3.932	39.9	93.87
Sb-20	6.961	34.36	49.34

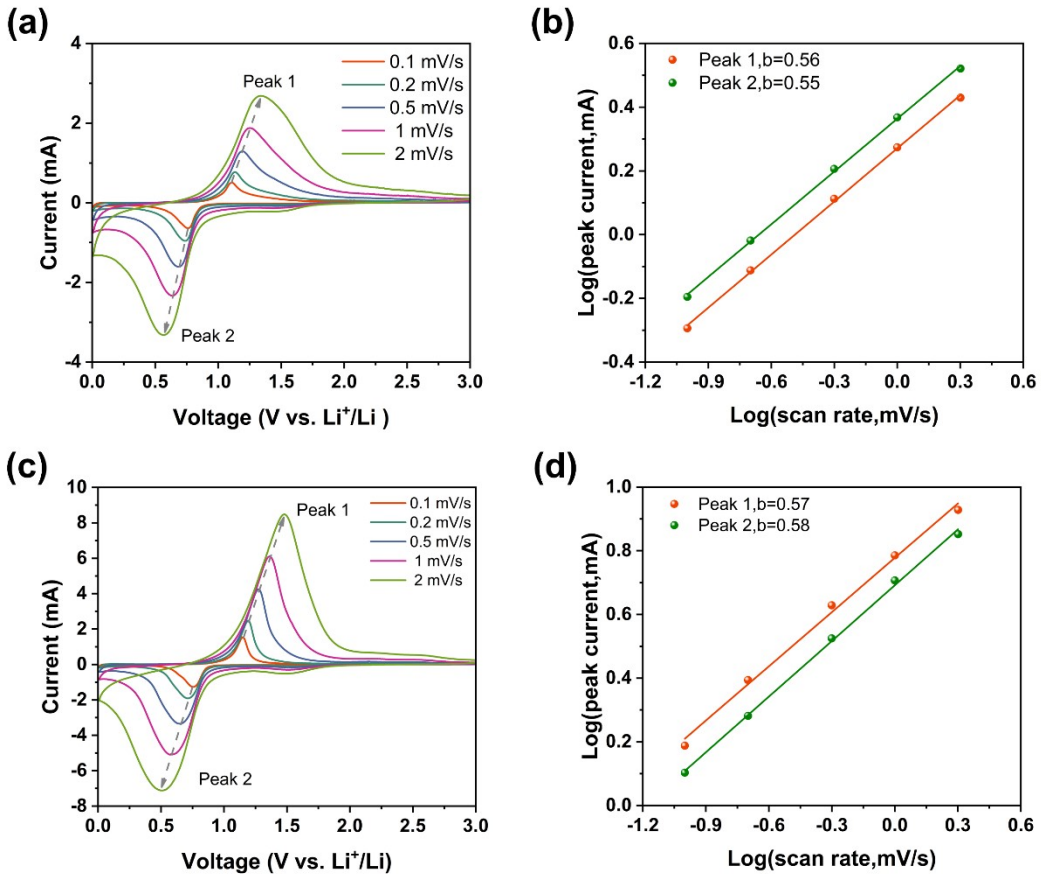

Figure S14. a) CV curves of Sb-15 at different scan rates and b) the corresponding plot of log(*i*) versus log (*v*). c) CV curves of Sb-30 at different scan rates. d) the corresponding plot of log(*i*) versus log (*v*).

Table S2. Fitting results obtained from the CV curves at various scanning rates.

	b-value (Peak 1)	b-value (Peak 2)
Bulk Sb	0.56	0.60
Sb-15	0.56	0.55
Sb-20	0.56	0.54
Sb-30	0.57	0.58

Table S3. The fitting results of the Bulk Sb (**Figure 3d**) according to $\ln[\ln(1/(1-f))] = \ln k + n\ln t$.

	Slope (n)	intercept (lnk)
30°C	0.96073	-3.65202
45°C	0.9192	-2.91602
60°C	0.82528	-2.64027

Table S4. The fitting results of the Sb-20 (**Figure 3d**) according to $\ln[\ln(1/(1-f))] = \ln k + n\ln t$.

	Slope (n)	intercept (lnk)
30°C	0.89368	-3.88621
45°C	0.936	-3.7077
60°C	1.12013	-3.42926

Table S5. The fitting results of the Bulk Sb (**Figure 3e**) according to $\ln[\ln(1/(1-f))] = \ln k + n\ln t$.

	Slope (n)	intercept (lnk)
30°C	1.00948	-1.24747
45°C	1.06934	-0.54102
60°C	1.03716	-0.28787

Table S6. The fitting results of the Sb-20 (**Figure 3e**) according to $\ln[\ln(1/(1-f))] = \ln k + n\ln t$.

	Slope (n)	intercept (lnk)
30°C	1.01209	-1.81878
45°C	0.98442	-1.61531
60°C	1.00638	-1.39809

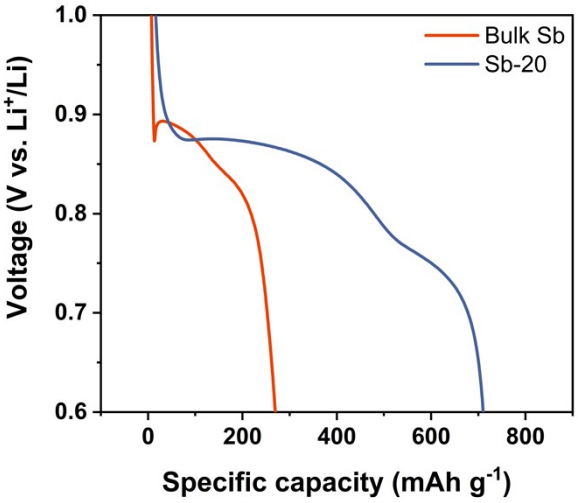

Figure S15. The voltage profiles of Bulk Sb and Sb-20 electrodes during discharge.

Table S7. The fitting results of the open-circuit potential *vs.* temperature for Bulk Sb and Sb-20 according to equation 8.

slope	Sb→Li_2Sb	Li_2Sb→Li_3Sb
Bulk Sb	0.00163	0.00473
Sb-20	8.14286E-4	0.00123

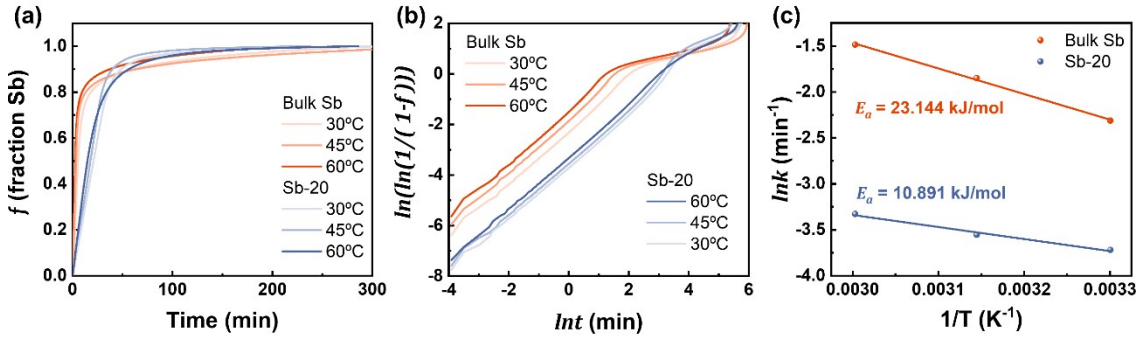

Figure S16. Phase transition kinetics of Bulk Sb and Sb-20 during lithiation. a) Volume fractions as a function of time, b) Plots of the $\ln[\ln(1/(1-f))]$ as a function of $\ln t$ for the formation of Sb and c) Arrhenius plots of the phase transition rate constants as a function of temperature for the two Sb electrodes.

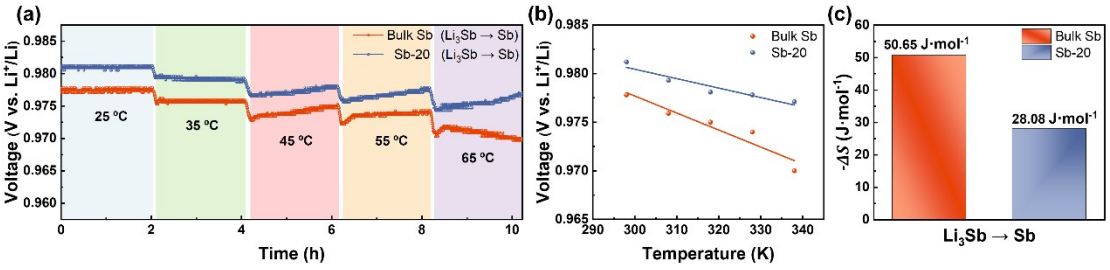

Figure S17. Thermodynamics of phase transitions during delithiation. a) Open-circuit potential variation with temperature. b) Linear fitting of the open-circuit potential as a function of temperature. c) Comparison of the entropy changes.